REPORT DOCUMENTATION PAGE

Form Approved
OMB No. 0704-0188

The public reporting burden for this collection of information is estimated to average 1 hour per response, including the time for reviewing instructions, searching existing data sources, gathering and maintaining the data needed, and completing and reviewing the collection of information. Send comments regarding this burden estimate or any other aspect of this collection of information, including suggestions for reducing the burden, to Department of Defense, Washington Headquarters Services, Directorate for Information Operations and Reports (0704-0188), 1215 Jefferson Davis Highway, Suite 1204, Arlington, VA 22202-4302. Respondents should be aware that notwithstanding any other provision of law, no person shall be subject to any penalty for failing to comply with a collection of information if it does not display a currently valid OMB control number.
PLEASE DO NOT RETURN YOUR FORM TO THE ABOVE ADDRESS.

1. REPORT DATE (DD-MM-YYYY)	2. REPORT TYPE	3. DATES COVERED (From - To)
21- 12-2006	Final Techical	19 Mar 2004 to 30 Sep 2006

4. TITLE AND SUBTITLE

Analysis and Modeling Using Multi-Year Satellite Observations in the Aegean and Eastern Mediterranean Seas

5a. CONTRACT NUMBER

5b. GRANT NUMBER

N00014-04-1-0380

5c. PROGRAM ELEMENT NUMBER

6. AUTHOR(S)

Kathryn Kelly

5d. PROJECT NUMBER

5e. TASK NUMBER

5f. WORK UNIT NUMBER

7. PERFORMING ORGANIZATION NAME(S) AND ADDRESS(ES)

Applied Physics Laboratory - University of Washington
1013 NE 40th Street
Seattle, WA 98105-6698

8. PERFORMING ORGANIZATION REPORT NUMBER

9. SPONSORING/MONITORING AGENCY NAME(S) AND ADDRESS(ES)

Office of Naval Research (322PO)
875 North Randolph Street, Suite 1425
Arlington, VA 22203-1995

10. SPONSOR/MONITOR'S ACRONYM(S)

11. SPONSOR/MONITOR'S REPORT NUMBER(S)

12. DISTRIBUTION/AVAILABILITY STATEMENT

DISTRIBUTION STATEMENT A
Approved for Public Release
Distribution Unlimited

13. SUPPLEMENTARY NOTES

NONE

14. ABSTRACT

Our objective was to understand how upper ocean processes, such as internal waves, seasonal-to-interannual variations of the circulation, eddy variability, SST, and wind forcing in the Aegean Sea affect mixing and temperature in the upper ocean.
An analysis of modeled and observed sea surface temperatures was submitted to the Journal of Geophysical Research – Oceans in October 2006 and is under review (abstract below). In addition, comparisons between the buoy winds and QuikSCAT in the Aegean Sea were used to optimize a mapping algorithm for the new higher-resolution (12.5 km) QuikSCAT winds. A relevant finding is that, for daily-averaged winds, mapped QuikSCAT winds are as accurate as an anemometer at about 100 km from a given location. This analysis is being incorporated in a manuscript describing the mapping algorithm and its verification in a manuscript in preparation.

15. SUBJECT TERMS

Internal waves, seasonal variations, SST, Aegean Sea, eastern Mediterranean Sea, QuikSCAT, SST

16. SECURITY CLASSIFICATION OF:			17. LIMITATION OF ABSTRACT	18. NUMBER OF PAGES	19a. NAME OF RESPONSIBLE PERSON
a. REPORT	b. ABSTRACT	c. THIS PAGE	UU	18	Kathryn Kelly
UNCLAS	UNCLAS	UNCLAS			19b. TELEPHONE NUMBER (Include area code) 206-543-9810

Standard Form 298 (Rev. 8/98)
Prescribed by ANSI Std. Z39.18

Analysis and Modeling Using Multi-Year Satellite Observations in the Aegean and Eastern Mediterranean Seas

Kathryn Kelly
Applied Physics Laboratory, Box 355640
University of Washington, Seattle, WA 98195
phone: 206-543-9810 fax: 206-543-6785   email: kkelly@apl.washington.edu
Award Number: N00014-04-1-0380
http://kkelly.apl.washington.edu/aegean

Final Report: December 2006

Our objective was to understand how upper ocean processes, such as internal waves, seasonal-to-interannual variations of the circulation, eddy variability, SST, and wind forcing in the Aegean Sea affect mixing and temperature in the upper ocean.

An analysis of modeled and observed sea surface temperatures was submitted to the Journal of Geophysical Research – Oceans in October 2006 and is under review (abstract below). In addition, comparisons between the buoy winds and QuikSCAT in the Aegean Sea were used to optimize a mapping algorithm for the new higher-resolution (12.5 km) QuikSCAT winds. A relevant finding is that, for daily-averaged winds, mapped QuikSCAT winds are as accurate as an anemometer at about 100 km from a given location. This analysis is being incorporated in a manuscript describing the mapping algorithm and its verification in a manuscript in preparation.

"Comparison of Modeled and Observed Sea Surface Temperatures in the Eastern Mediterranean and Aegean Seas" by Kathryn A. Kelly

A column mixed layer model is run for the Aegean and eastern Mediterranean Seas and results are compared with SST and for the autumns of 2001-2004 to determine whether errors in modeling SST can be attributed to missing model physics, primarily mixing. Discrepancies between the modeled and observed SST were found to be about the same size as differences between SST products, so that model errors could not be definitively isolated. However, much canbe learned about the accuracy of the forcing and observed fields from this study. SST fluctuations with temporal scales of 10--14 days were determined to be caused by latent heat flux variability, which is somewhat underestimated by the second NCEP/NCAR Reanalysis (NCEP2)fluxes. Spatial variations in air-sea fluxes on spatial scales not resolved by the Reanalysis, as determined by comparisons between NCEP2 and scatterometer winds, substantially degrade model performance. Contributions from advection are relatively small. Biases in the NCEP2 precipitation-minus-evaporation fields cause systematic errors in mixed layer depth and in temperature. Relaxing the salinity to climatological values, combined with small bias corrections to air-sea fluxes gives better agreement with observed SST. Model performance was judged by comparing observed and modeled temperature tendency, a more stringent comparison than with SST; good results were obtained in the eastern Mediterranean and Aegean Seas, but not in the central Mediterranean. A relatively poor match with an infrared-based SST product is apparently caused by cloud-contamination, not the mixed layer model, a result established by comparisons with microwave SST and cloud cover.

Comparison of Modeled and Observed Sea Surface Temperatures in the Eastern Mediterranean and Aegean Seas

Kathryn A. Kelly

Applied Physics Laboratory, University of Washington, Seattle, Washington, USA

Abstract. A column mixed layer model is run for the Aegean and eastern Mediterranean Seas and results are compared with SST and for the autumns of 2001-2004 to determine whether errors in modeling SST can be attributed to missing model physics, primarily mixing. Discrepancies between the modeled and observed SST were found to be about the same size as differences between SST products, so that model errors could not be definitively isolated. However, much can be learned about the accuracy of the forcing and observed fields from this study. SST fluctuations with temporal scales of 10–14 days were determined to be caused by latent heat flux variability, which is somewhat underestimated by the second NCEP/NCAR Reanalysis (NCEP2) fluxes. Spatial variations in air-sea fluxes on spatial scales not resolved by the Reanalysis, as determined by comparisons between NCEP2 and scatterometer winds, substantially degrade model performance. Contributions from advection are relatively small. Biases in the NCEP2 precipitation-minus-evaporation fields cause systematic errors in mixed layer depth and in temperature. Relaxing the salinity to climatological values, combined with small bias corrections to air-sea fluxes gives better agreement with observed SST. Model performance was judged by comparing observed and modeled temperature tendency, a more stringent comparison than with SST; good results were obtained in the eastern Mediterranean and Aegean Seas, but not in the central Mediterranean. A relatively poor match with an infrared-based SST product is apparently caused by cloud-contamination, not the mixed layer model, a result established by comparisons with microwave SST and cloud cover.

1. Introduction

Sea surface temperature (SST) variations are a complicated response to air-sea heat and freshwater fluxes, wind, mixing, and advection. In a region as complex geographically as the Mediterranean Sea one expects these processes to have different balances in different regions. In particular, higher levels of mixing associated with internal waves, tides, or other geographically correlated processes may produce temperature anomalies that are not predicted by simple mixed layer models. Conversely, systematic errors between observed and modeled temperatures may indicate the location and extent of anomalous mixing processes. More generally, given sufficiently accurate forcing fields and observations for comparison, the question addressed here is: Do temperature errors indicate missing model physics?

This study was motivated by a workshop on the Aegean Sea, sponsored by the U.S. Office of Naval Research [*Sofianos et al*, 2002], and a field program, of which one of the goals is to understand the contributions of tides and internal waves to ocean mixing. Particularly in the fall when thermal stratification is large, internal waves and tides would be expected to increase

vertical mixing and to decrease SST. Related scientific questions raised in the workshop report include: How is the wind stress pattern affected by the presence of complex orography? How do the resulting patterns of surface wind stress around the islands affect eddies, internal waves, and mixing? What are the patterns and dominant processes affecting oceanic convection and re-stratification? How are these processes modulated by islands, plateaux, and eddies? While these questions can only be conclusively answered in conjunction with extensive field measurements and concurrent modeling studies, an analysis of the increasingly accurate forcing fields and observations currently available may give a useful overview and assist in designing more detailed studies.

Several large-scale processes that likely influence temperatures in different regions of the Mediterranean and Aegean Seas have been investigated using field programs and numerical studies. Sea level has been rising in the Mediterranean Sea, as observed by the TOPEX/Poseidon radar altimeter [*Cazenave et al.*, 2001], particularly in the region east of Crete; SST and hydrographic data show corresponding increases in water temperature. A recent study by *Fukumori* [2006] showed that the Mediterranean Sea has a relatively rapid and nearly uniform barotropic (seiche-like) response to wind stress with time scales of weeks to months, based on model experiments and altimeter data. A possible influence of the wintertime North Atlantic Oscillation has been found in the circulation of the Western Mediterranean Sea [*Vignudelli et al.*, 1999], based on a time series of currents in the Corsica Channel. A numerical simulation of circulation by *Pinardi et al.* [1997] showed that the Eastern Mediterranean Sea has considerably more interannual variability than the Western Mediterranean. Unlike in the west, strong wintertime winds and heat fluxes in the Eastern Mediterranean can modify the ocean circulation and structure to overcome the normal seasonal cycle the following summer. Quasi-stationary and recurrent eddies have been observed in the eastern Mediterranean Sea using aerial surveys and drifting buoys [*Matteoda and Glenn*, 1996].

Against this background of regional variations in ocean and forcing variability, the ability of a well-known mixed layer model to simulate sea surface temperatures (SST) is evaluated for the eastern Mediterranean Sea (Levantine and Ionian Basins) and for the Aegean Sea. The Price-Weller-Pinkel [*Price et al.*, 1986] mixed layer model is used here, forced by new air-sea flux and wind products. Several air-sea flux products are evaluated to determine their effectiveness; the model results are then compared with two new SST products. In addition, there are some in situ temperature and wind observations available for comparison in the Aegean Sea, as well as some visible images of the region from the MODIS. Analyses of observations showing regions of high variability are presented in Section 2. Section 3 gives the methodology, including the model set up, and the adjustments to the forcing fields. In Section 4 the model and observations are compared, and the sensitivity of the model to forcing is examined. The summary and conclusions are presented in Section 5.

2. Evaluation of Observations and Forcing

Several, primarily satellite, data sets were examined to provide information on regional variability, including the existence of internal waves, the effects of topography on winds, and temperature variations. Both temperature and wind accuracies were evaluated by comparisons with observations from a network of buoys in the Aegean Sea, maintained by the Hellenic Centre for Marine Research.

2.1. Satellite Observations of Internal Waves

To determine the effect of internal waves on ocean mixing, it would be useful to have a statistical description of when and where internal waves occur. Internal waves have been observed using a variety of sensors [*Global Ocean Associates*, 2004], including an imaging radar on the Space Shuttle. Two sources of data exist from which a statistical description might be obtained: high-resolution visible images and synthetic aperture radar (SAR) images.

True color (visible) images from MODIS (Figure 1a) on either the Aqua or Terra satellites are readily available with a resolution of about 250m from NASA's Goddard Space Flight Center. Modulations of the ocean surface roughness can only be seen when highlighted by sunglint in cloud-free regions; sun-ocean surface viewing geometry limit the useful observation period to the months of June, July, and August. All available data (64 images) from both platforms for 2002–2004 were examined. During this period, there were no obvious examples of internal waves in the eastern Mediterranean or Aegean Seas; however, there are no objective ways to determine whether the observed signatures are caused by the atmosphere or by processes internal to the ocean.

Browse images of SAR data from the European Space Agency were also examined. SAR data is not restricted by viewing geometry or clouds. Again, there were no clear examples of internal waves in the SAR images, and recent studies that suggest that no algorithm exists to extract the signature of internal waves in the presence of

many other types of oceanographic phenomena [*Ivanov*, 2002].

Nevetheless, the MODIS images provide useful information about variability in the region. Bright patches are observed (Figure 1a) on the south side of Crete and the numerous islands in the Aegean Sea in about 70% of the images,usually during periods of strong (southward) winds. Wave or eddy-like surface patterns occur in about 50% of the images, usually in a location near the edge of the sunglint, suggesting that these features may be obscured by the bright patches that appear under high-wind conditions.

2.2. Wind Fields

High-resolution data from the SeaWinds scatterometer on QuikSCAT (Figure 1b) reveal topographically modified wind fields that resemble wakes on the downwind side of islands [*Chelton et al.*, 2004]. The bright patches in MODIS images (Figure 1a) likely represent a sea surface response to the winds: wind shielding by island topography results in a smoother ocean surface that in turn reflects more sunlight, producing the bright patches in the MODIS images. Such high-resolution wind fields offer the potential for improved modeling of ocean processes. Correlations between the buoy winds and collocated 12.5km-resolution QuikSCAT winds are typically 0.8–0.9. To force an ocean model, the original swath-oriented wind vectors must be gridded at a lower resolution, consistent with the revisit time of the satellite (about 12 hours). At the time of this study, the high-resolution QuikSCAT winds shown here were only available for calendar year 2003. Therefore, the winds used in the modeling study were the standard 25-km winds, objectively mapped to a $1° \times 1°$ grid with approximate 4-day resolution (to maintain consistent data quality, *Kelly et al.* [1999]). Despite the high degree of smoothing, correlations with buoy winds do not drop dramatically with gridding: correlations between buoy and the gridded winds are typically 0.75-0.8. A detailed evaluation of the high-resolution winds and the effects of gridding, relative to the winds from the buoys, will be the subject of a future report.

The gridded QuikSCAT $1° \times 1°$ wind products have considerably higher spatial resolution than most currently available numerical weather prediction products, such as NCEP2 (see Section 4.3). While improved resolution in wind stress and wind stress curl would likely give improvements in dynamical models, wind stress makes a relatively small contribution to the variability of the mixed layer model, for which the dominant forcing is the air-sea flux. A recent study by *Jiang et al.* [2005] suggests that combining QuikSCAT winds
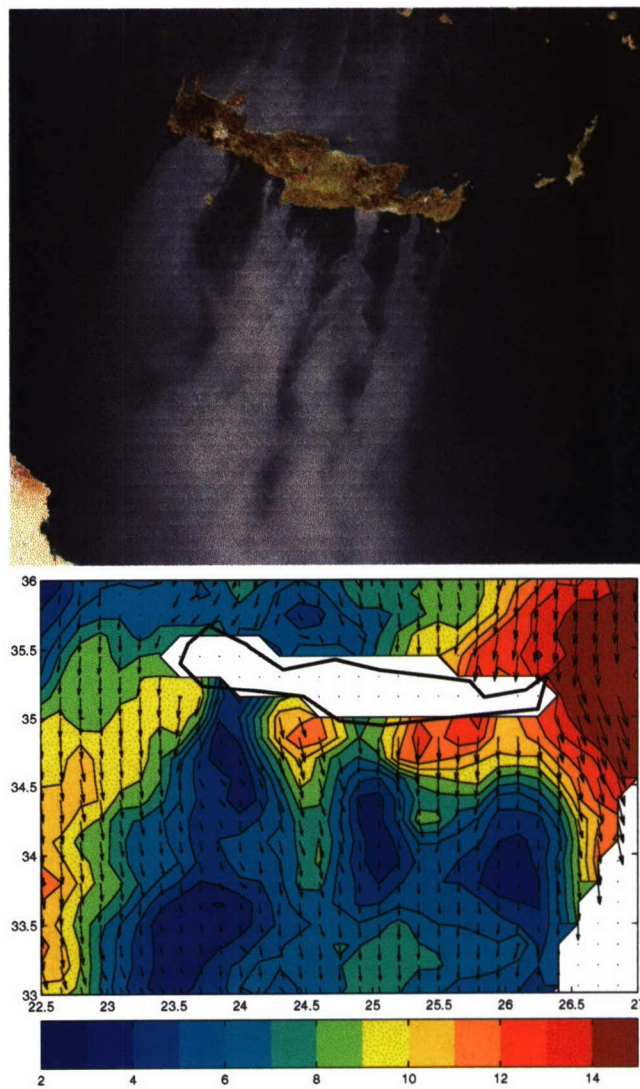
Figure 1. Island wakes on the leeward (south) side of Crete on 28 July 2003. (a) MODIS true-color image from Aqua at 1120 UTC and (b) high-resolution QuikSCAT wind vectors at 1700 UTC. Color contours are wind speed with contour interval of 1 m s^{-1}. Low wind speeds in (b) correspond to lighter colors in (a).

and satellite SST with lower-resolution air temperature and humidity produces an improved flux product in the equatorial Pacific, where latent heat fluxes clearly dominate, but this may not be true for other regions. To take full advantage of the improved resolution in winds (and SST) for heat fluxes, air temperature and humidity would also need to be available at higher spatial resolution. An estimate of the magnitude of the errors induced by poor spatial resolution in the flux fields is included in Section 4.3, using the region south of Crete.

2.3. Sea Surface Temperature (SST)

Two SST products are used in the evaluation of the model performance (Figure 2). The first is a relatively new product from the National Centers for Environmental Prediction (NCEP), designated Real Time Global (RTG). Although it is derived from the same infrared sensors that are used for the standard "Reynolds" [*Reynolds et al*, 1994] SST, the spatial resolution of the RTG SST is much higher. The second SST product used here is an optimally interpolated version of microwave SST (from the TRMM Microwave Imager) available from Remote Sensing Systems. Because microwave sensors can measure through clouds, unlike infrared sensors, the microwave SST products are potentially more accurate, particularly in regions of persistent cloud cover. Disadvantages of the microwave sensors are that it has inherently lower spatial resolution ($\approx$ 50 km) and that any land within its relatively large field-of-view renders the data unusable. Thus, microwave SST is not reliable in most of the Aegean Sea or near any coastline.

Before evaluating the ability of a model to reproduce observed mixed layer temperatures, the SST products were first compared with temperatures from buoys in the Aegean Sea at 3 meters below the surface at 3-hr intervals (See Figure 3 for buoy locations). The comparison time period was from January 2001 to mid-May 2004. Microwave SST was available at only the two southernmost buoys. For these two buoys, RTG SST had a negligible bias of about 0.2°C, whereas TMI SST had a bias of approximately 1.5°C. Correlations between SST and buoy temperatures were examined after first removing the seasonal cycle (once and twice per year harmonics); correlations for all SST series were statistically significant with RTG values of 0.50 and 0.49 and TMI values of 0.61 and 0.46. The proximity of land throughout the Aegean Sea likely degrades the TMI SST in the buoy comparisons and causes a warm bias. In the central Mediterranean, TMI appears to be more accurate than RTG (see Section 4.1, below).

The quantity used to determine how well the PWP
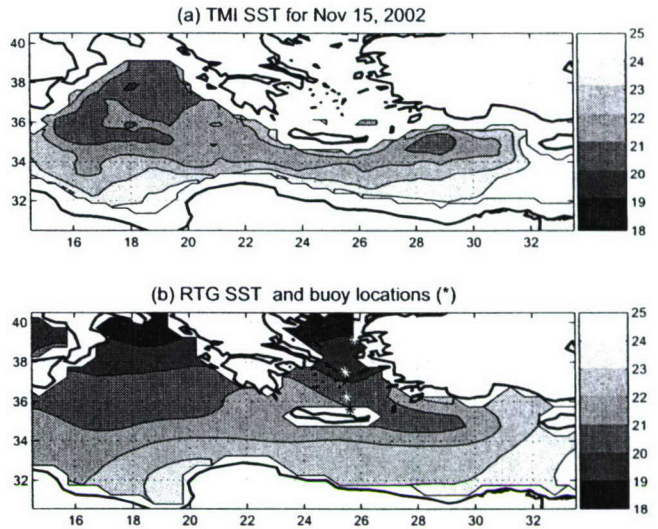
Figure 2. Maps of SST products for 17 October 2001. SST maps derived from (a) the microwave sensor TMI and (b) the high-resolution NCEP RTG product. Locations of three buoys in the Aegean Sea used to evaluate satellite fields shown as asterisks. Buoys are named after nearby islands: from south to north, Avgo, Santorini, and Mykonos.

model performed was actually temperature tendency, $\partial T/\partial t$, rather than temperature itself because it is the rate of temperature change that is directly related to the forcing. Therefore, this quantity was also compared between SST and the 3-m temperatures (Figure 4). A slight modification was necessary for the TMI data to increase the accuracy of $\partial T/\partial t$. Because the mapped TMI data are used in near real time, the interpolation algorithm uses only data from previous times. In the relatively rare event of missing data owing to rain, SST from the previous clear period is used, resulting in an unrealistically high occurrence of zeroes in the value of $\partial T/\partial t$. Therefore, wherever $\partial T/\partial t$ was found to be exactly zero, the temporally constant SST values were replaced by a linear interpolation between previous and subsequent SST estimates.

To estimate a sensible value for temperature tendency, it is necessary to smooth the SST fields temporally to reduce errors in the SST products, while retaining the highest frequency variations actually resolved by the fields. To determine an appropriate temporal lowpass filter to apply to the SST data, correlations were computed between temperature tendency from SST and from daily averaged 3-m buoy temperatures, after applying a series of lowpass filters with half-power periods from 4 to 12 days. Correlations between the two filtered series of $\partial T/\partial t$ increased steeply up to periods
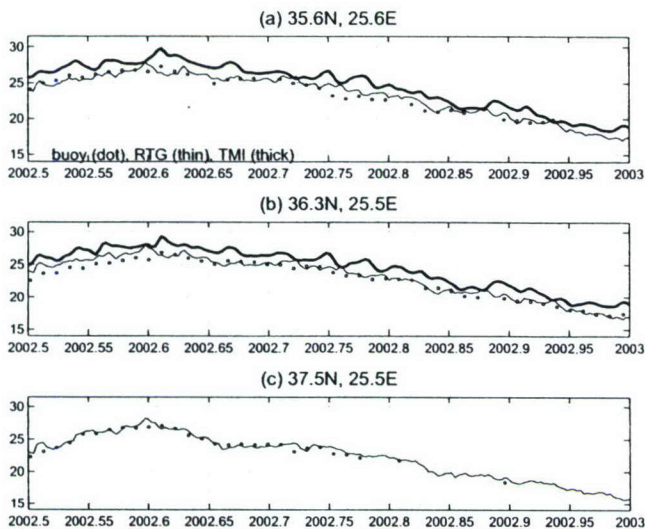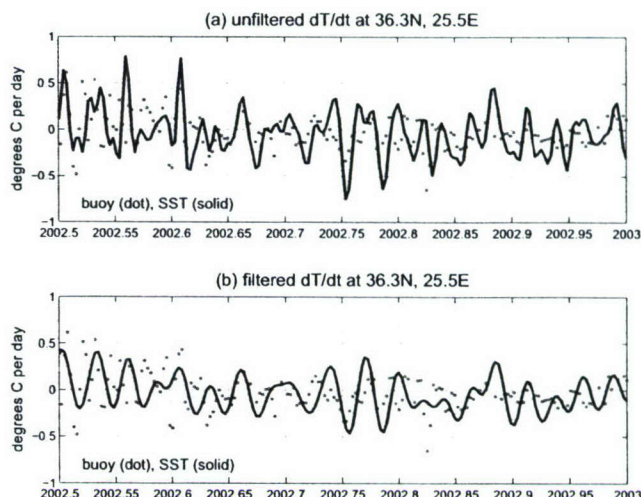
Figure 3. Comparison of SST products with buoy temperatures. Time series at the three southernmost buoy locations shown in Figure 2a for the second half of 2002. TMI SST (thick line), RTG SST (thin line) and 3-m buoy temperatures (dots).

Figure 4. Temperature tendency of SST and buoys. (a) Time series of $\partial T/\partial t$ at Santorini (compare Figure 3b) for the second half of 2002 for RTG SST (solid line) and 3-m buoy temperatures (dots). (b) Lowpass filtered tendency for RTG SST with half-power of 9 days. Tendency from buoys repeated for comparison.

of approximately 8–10 days (indicating a reduction in SST errors) and then remained relatively flat with increasingly longer periods. This analysis suggests that SST fluctuations with periods less than about 9 days are dominated by errors in the SST maps or are associated with the skin temperature of the ocean. There are energetic fluctuations in the buoy temperatures with periods shorter than 9 days, but these fluctuations are not resolved by the SST products. In comparisons with the model, all SST data have been lowpass filtered with a half-power period of 9 days.

2.4. Air-Sea Heat Fluxes

The model was forced by air-sea heat fluxes and precipitation-minus-evaporation (or freshwater fluxes), primarily from the second NCEP/NCAR Reanalysis (NCEP2) [*Kistler et al.*, 2001]. Different combinations of radiative and turbulent heat fluxes were used to force the model, including both NCEP2 radiative and turbulent heat fluxes, and radiative fluxes from the International Satellite Cloud Climatology Project [*Zhang et al.*, 2003]. An additional set of latent and sensible heat flux fields were derived by using the NCEP2 variables in the COARE algorithm [*Fairall et al.*, 1996], version 3.0. The PWP model also requires wind stress (for horizontal momentum) and wind stress curl for calculating vertical velocity and vertical diffusion. Gridded QuikSCAT wind stress and wind stress curl fields were used to force the model; however, as discussed in Section 4.2, the re-

sults are relatively insensitive to the accuracy of these products.

Several heat flux products were compared and tested for their ability to simulate mixed layer temperature in the PWP model. The flux components are first examined separately: radiative fluxes (shortwave and longwave) and turbulent fluxes (latent and sensible). The oceanographic convention is used here, that is, positive fluxes represent heat fluxed into the ocean. Radiative fluxes include daily fields from NCEP2 and daily fields from ISCCP. Turbulent fluxes include the NCEP2 product as well as a flux product derived by using daily NCEP2 atmospheric variables in the COARE algorithm.

Mean values over 2001–2004 were compared for each flux component and product. Shortwave radiative fluxes from NCEP2 are on average about $20 \mathrm{Wm}^{-2}$ stronger than the ISCCP fluxes (Figure 5), which incorporate cloud forcing from observations. Longwave fluxes (not shown) are comparable in magnitude. NCEP2 turbulent fluxes are also compared with the NCEP2/COARE fluxes. Latent heat flux products (Figure 6) differ by about $20 \mathrm{Wm}^{-2}$ overall, with NCEP2 more negative, except near the northern coast of Africa, where the influence of land appears to make the NCEP2 fluxes change abruptly to values less negative than in the central Mediterranean by more than $30 \mathrm{Wm}^{-2}$. Sensible fluxes (not shown) are comparable in magnitude over the ocean, with large gradients also near the coast of
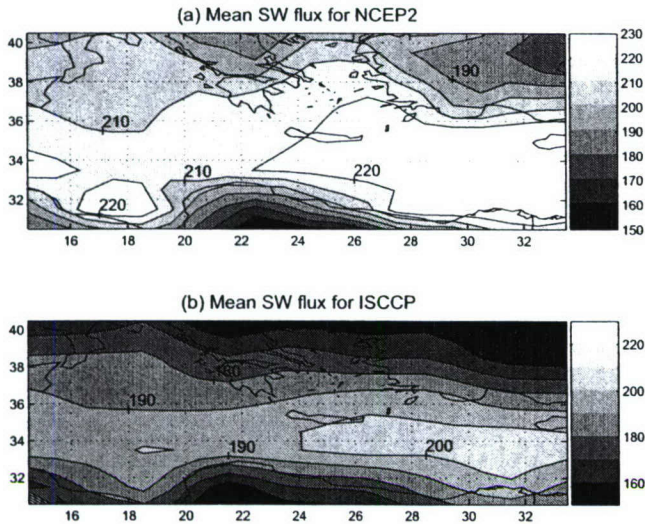
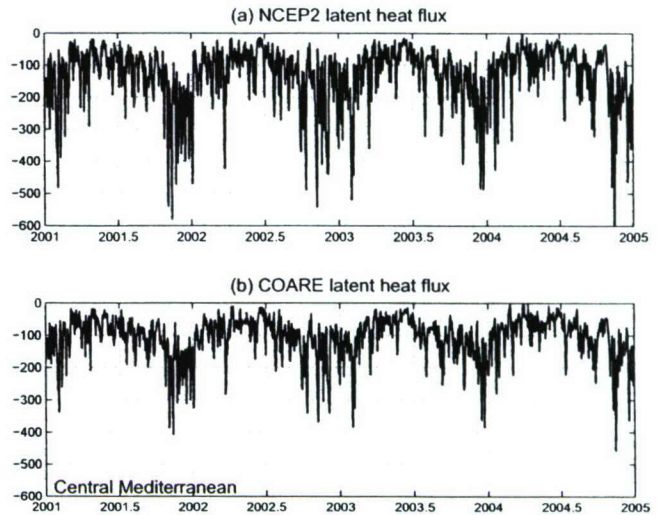**Figure 5.** Comparisons of shortwave fluxes for 2001–2004. (a) Mean shortwave flux from (a) NCEP2 and (b) ISCCP. Units are Wm^{-2}.
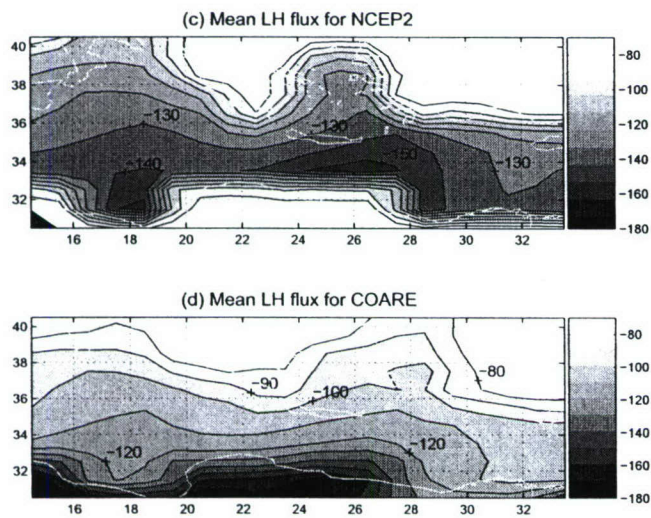
Figure 6. Comparisons of latent heat fluxes for 2001–2004. (a) Mean latent heat flux from (a) NCEP2 and (b) COARE. Units are Wm^{-2}.

Figure 7. Time series of latent heat flux for 2001–2004 in the Central Mediterranean. Daily latent heat flux from (a) NCEP2 and from (b) NCEP2 variables used in the COARE algorithm. Units are Wm^{-2}.

Africa. Interestingly, the stronger mean shortwave and stronger mean latent heat fluxes in NCEP2 nearly cancel in the net heat flux to give net fluxes about the same as the sum of ISCCP plus COARE fluxes.

Much larger differences are seen when examining the time series of daily averaged latent heat flux at a particular location, for example, at 34.5°N, 14.5°E (Figure 7). The standard deviation of latent heat flux is about 40% larger in NCEP2 than in the COARE product. Maxi-

mum wintertime heat losses from the COARE flux are about $400Wm^{-2}$, whereas NCEP2 maximum heat loss exceeds $500Wm^{-2}$. Some reduction in the magnitudes could be the result of nonlinearity in the bulk algorithm, as daily averages of the NCEP2 variables are used; however, *Jiang et al.* [2005] showed that the nonlinearities are small, at least for the tropical Pacific. These differences would be expected to produce substantial differences in wintertime SST. The larger NCEP2 anomalies occur throughout the study region.

Over most of the ocean few objective measures exist to evaluate absolute flux product accuracy. However, in the Mediterranean Sea a recent study by *Krahmann et al.* [2000] uses the ocean heat budget to infer the seasonal cycle of net surface heat fluxes (with error bars) and evaluate several products. Temporal changes in ocean heat content are the sum of the net surface heat fluxes and the ocean heat transport divergence; therefore, to obtain an estimate of absolute net surface heat fluxes they subtract from the time derivative of the seasonal cycle of ocean heat content (down to the bottom of the ocean) an estimate of the seasonal cycle of the heat transport through the Strait of Gibraltar. To compare the heat flux products with the estimates of *Krahmann et al.* [2000] each version of the net fluxes was averaged over the entire Mediterranean Sea and from each was extracted a single annual harmonic for the four-year series (Figure 8). This estimate of the NCEP2 seasonal net heat flux agrees well with estimates from *Krahmann et al.* [2000]: a maximum flux of 166
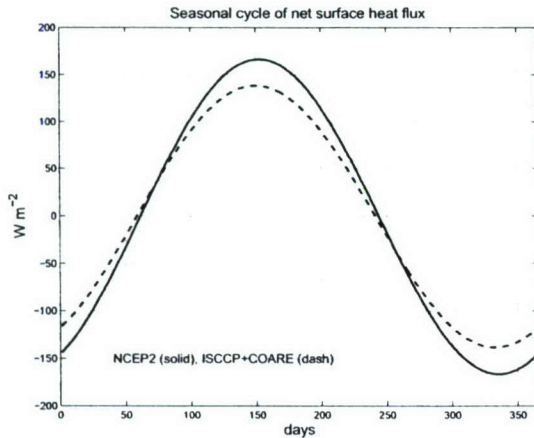
Figure 8. Annual cycle of net surface heat flux for 2001–2004 averaged over the entire Mediterranean Sea. Net surface heat flux from NCEP2 (solid) and ISCCP plus COARE (dash). Units are Wm^{-2}.

Wm^{-2}, compared with a range of acceptable values of 145 to $170Wm^{-2}$, and a minimum of about $-167Wm^{-2}$, compared with -160 to $-185Wm^{-2}$. The combined IS-CCP plus COARE seasonal net heat flux has a smaller seasonal range of fluxes than does NCEP2. Although the ISCCP/COARE maximum value of $144Wm^{-2}$ lies nearly within the specified range of 145 to $170Wm^{-2}$, its minimum value of $-135Wm^{-2}$ is well outside the *Krahmann et al.* [2000] minimum range.

3. Methodology

3.1. Mixed Layer Model

The model used in this study is the Price-Weller-Pinkel (PWP) mixed layer model [*Price et al.*, 1986]. The model was run as a column with 2-m vertical resolution to a depth of about 450 m at each point in a $1° \times 1°$ grid, that is, neglecting input from adjacent grid points. However, some experiments were performed to estimate the effect of advection using observed currents and SST gradients. The PWP model yields Ekman velocities and these are used in some of the experiments testing the contribution of horizontal advection. The vertical profile of shortwave irradiance was based on values for Type 1A water ($R=0.62$ and $\gamma=20$). The PWP model uses both a gradient and bulk Richardson number for convection; the critical values for overturning were set at 0.65 and 0.25, respectively. Vertical diffusivity was set at 5×10^{-5} m s^{-1}.

The model was initialized using temperature and salinity profiles derived from the World Ocean Database (2001) [*Conkwright et al.*, 2002] climatology in mid-

October of each year and was then run using daily forcing fields interpolated to match the 6-hr time step. The model was run for periods of three months beginning in mid-October of the years 2001, 2002, 2003, and 2004. The fall was selected as a time when vertical mixing processes would have a large impact, owing to strong stratification and relatively shallow mixed layers. The mid-October start time was selected to avoid the shallowest mixed layers in which small errors in depth have a large effect on mixed layer temperature.

Trends toward higher temperatures and salinities in the Mediterranean Sea [*Cazenave et al.*, 2001; *Krahmann and Schott*, 1998] made it necessary to adjust climatological values using observed SST. To distinguish changes in the water column from changes confined to the surface, SST was compared with climatological SST at each grid point for March, the month corresponding to the deepest mixed layers. Observed temperatures were typically higher than climatological SST by 0.5–1.0°C. A single adjustment for the 4-yr period was made by adding the mean March SST difference to the surface temperature and tapering it linearly to zero at 600-m depth. A similar adjustment was made to climatological salinity, using a regression between temperature and salinity to infer the T-S relationship; salinity adjustments were negligible compared with the seasonal cycle of salinity variations. In addition to the adjustment to climatological T and S for a warming ocean, for each model run at each grid point, SST was used to adjust the initial temperature profile, but only down to the depth of the wintertime mixed layer. Salinity was not adjusted further.

Daily fields of shortwave flux, longwave plus turbulent fluxes, wind stress, wind stress curl and freshwater flux were used to force the PWP model, after interpolation to the 6-hr model time step. Two versions of the net surface heat flux were used: the sum of all four NCEP2 fluxes and the NCEP2 radiative fluxes combined with the NCEP2/COARE turbulent fluxes.

In the initial runs with the prescribed forcing, the most noticeable discrepancies with climatological values were a tendency for the water column to be too saline and the mixed layer to be too deep. Climatological salinity shows a tendency to decrease (freshening of the water column) presumably in response to seasonal rainfall over the October–January period, whereas the NCEP freshwater fluxes are typically negative over this period (an excess of evaporation). To create a more realistic model response to forcing, a simple bias correction was made to both the freshwater and heat fluxes. The bias corrections help maintain both a mixed layer depth (MLD) that more closely resembles climatology

and gives better agreement with the observed seasonal trends of SST.

3.2. Heat Flux Corrections

Two methods for adjusting the net surface heat flux were examined using the NCEP2 fluxes. The first adjustment was based on the difference between observed and modeled SST: a straight line was fit to the time series of the observed SST minus model SST. A heat flux adjustment was estimated as $q_{adj} = m\rho c_p <h>$, where m is the tendency of the SST error in $°C$ s^{-1}, c_p is the specific heat of seawater, and $<h>$ is the mean climatological MLD. The second method compared modeled and climatological heat content (the vertical integral of temperature), to eliminate the effect of vertical entrainment on SST. In this case a heat flux adjustment was estimated as $q_{adj} = \alpha m\rho c_p$, where m is now the tendency of the heat content difference in m$°C$ s^{-1} and α was set to 0.3, to allow for interannual departures from climatology. The magnitude of the correction was generally less than 30Wm^{-2} for either method. Corrections based on SST tended to be negative (less heat into the ocean), whereas corrections based on heat content tended to be positive. The need to provide more cooling in the mixed layer to match observed SST, while the heat content in the water column was apparently decreasing too fast suggests that the model mixed layers are slightly too deep.

Corrections to the surface heat fluxes vary considerably (Figure 9) regionally and temporally; corrections shown were derived from the SST-based adjustment. The value of the correction is relatively small compared with the net flux; corrections are typically less than 30Wm^{-2}. For the SST-based method, the flux corrections using both the RTG and TMI versions of SST were compared (not shown); the corrections are qualitatively similar and are about the same magnitude. Again using the SST-based method, NCEP2 net fluxes were compared with NCEP2 radiative plus NCEP2/COARE turbulent fluxes. Although bias corrections differed between products by as much as 30Wm^{-2}, the bias magnitudes were again less than about 30Wm^{-2}.

An analysis of the heat budget in the Aegean Sea [Poulos et al., 1997] gives a climatological net surface heat flux of approximately -26Wm^{-2}, a small heat loss to the atmosphere that is compensated by warm water advection. In the PWP runs (in which advection is neglected) one would expect a surface heat flux correction of about this size. However, the flux corrections in the Aegean Sea using SST have no consistent sign, whereas the flux corrections based on heat content are positive, suggesting that the flux biases are not the result of a
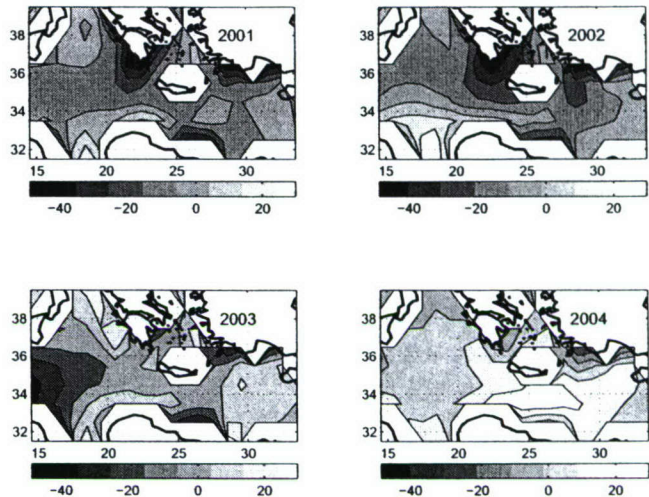

Figure 9. Heat flux corrections. Net surface heat flux at each grid point was adjusted to match the mean temperature tendency to observed values from the RTG SST by adding a constant offset to the fluxes from NCEP2 for each year. Units are Wm^{-2}. Corrections were typically less than 30 Wm^{-2}.

neglect of advection.

3.3. Freshwater Flux Corrections

In contrast to the relatively small heat flux corrections, freshwater fluxes required corrections as large as the flux itself. On average freshwater fluxes from NCEP2 are negative over the three-month model period, causing the water column salinity to increase, whereas climatological salinity decreases in the fall. An analysis of climatological fluxes in the Aegean Sea shows that precipitation exceeds evaporation from November through January [Poulos et al., 1997].

To compute the freshwater flux correction after the initial run with prescribed fields, the model salinity profile $S(z)$ at the end of the run is compared with the January climatological profile, both vertically averaged to the maximum climatological mixed layer depth for October–January. An empirical adjustment is added to the mean freshwater flux to improve the match with climatological salinity. The freshwater flux corrections (Figure 10) are generally positive (except in the Adriatic Sea), and typically reverse the sign of the average flux over the three-month period from negative to positive to reduce the modeled salinity, consistent with the climatological tendency. Biases in the salinity tend to make the mixed layer too deep and therefore suppress higher-frequency changes in the surface temperature, particularly early in the model run; these adjustments
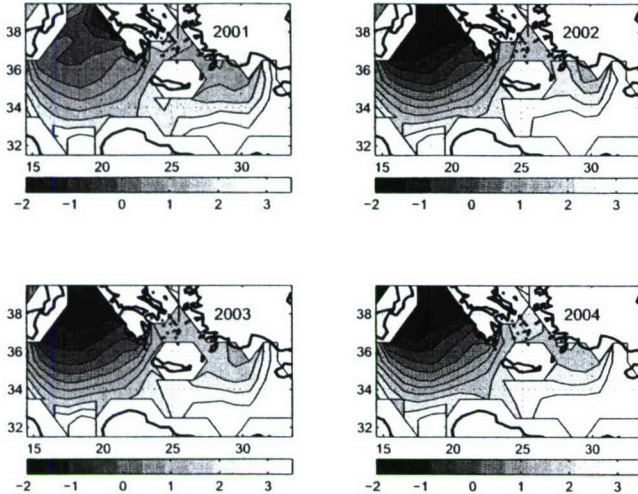
Figure 10. Freshwater flux corrections. Salinity at each grid point was relaxed toward climatological salinity by adding a constant offset to the freshwater fluxes from NCEP2 for each year. Units are $m\,y^{-1}$.

generally make the mixed layer more shallow, consistent with climatological MLD.

The freshening of the water column and the need to apply a freshwater flux correction may be owing in part to neglect of the inflow from adjacent bodies of water, as well as from numerous rivers. For example, in the Aegean Sea it has been estimated that evaporation would exceed precipitation plus river inflow, on average, but an inflow of fresh water from the Black Sea creates a net freshening (positive flux) [*Poulos et al.*, 1997].

After estimating both the freshwater and heat flux corrections, the model was re-run with the adjusted fluxes (Figure 11). The constant heat flux correction generally had a negligible direct effect on the temperature tendency, which was dominated by variability on time scales of 1-2 weeks. The freshwater flux correction consistently gave a shallower mixed layer (closer to climatology) and improved the comparisons with observed temperature tendency, as discussed below.

4. Comparison of Model and Observations

4.1. Correlations with Observed Tendency

To quantify model accuracy, at each grid point for each year, correlations were computed between temperature tendency $\partial T/\partial t$ for the model and the observed SST (Figure 12). Using the RTG SST product, which covers more of the study region, correlations are above the 95% significance level (typically 0.35) over much of
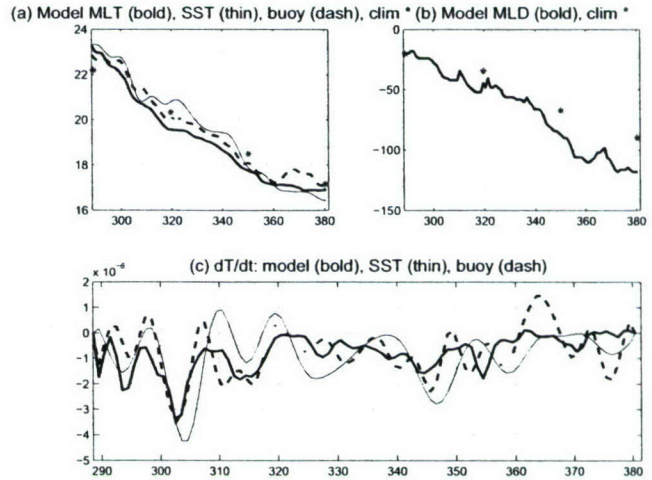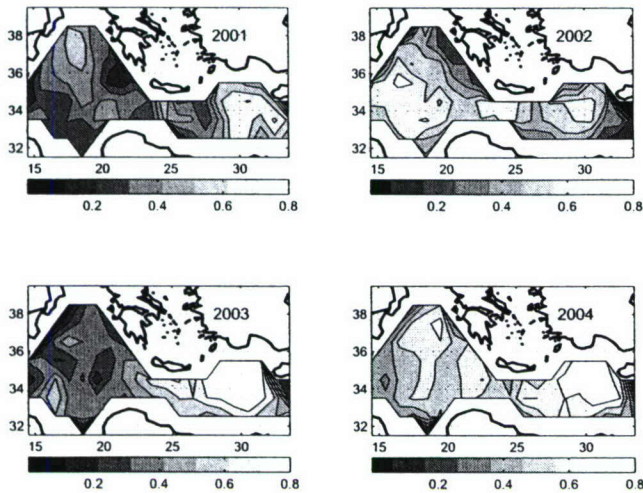

Figure 11. Observed and modeled variables at the Santorini buoy at 36.3°N, 25.5°E in the fall of 2002. (a) RTG SST (thin line), 3m buoy temperature (dash), and model (thick) and climatological mixed layer temperature (*). (b) Modeled (thick) and climatological mixed layer depth (*). (c) As in (a), but temperature tendency $\partial T/\partial t$.
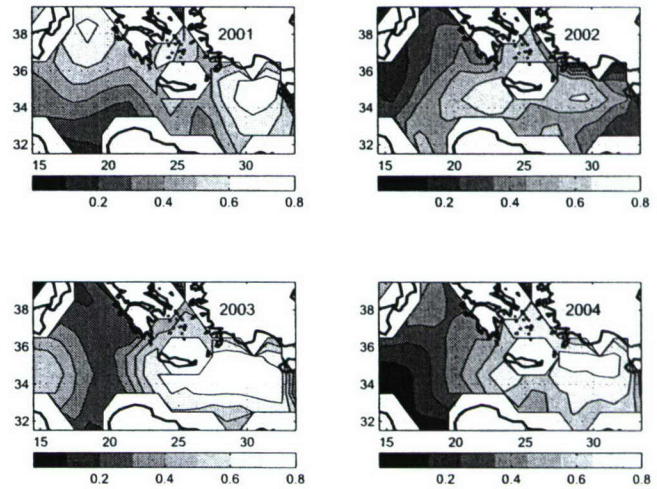
Figure 12. Evaluation of model mixed layer temperature. Correlations between temperature tendency $\partial T/\partial t$ from model and from RTG SST for each year.

the region in all years. The region with the lowest correlations (mixed layer temperature tendency least resembles that from the RTG SST) is the central Mediterranean, west of about 20°E.

Correlations vary from year to year, suggesting that the model's physics (or its forcing fields) may vary in accuracy. For example, in the eastern Mediterranean, correlations are above 0.6 in each year except for 2002.
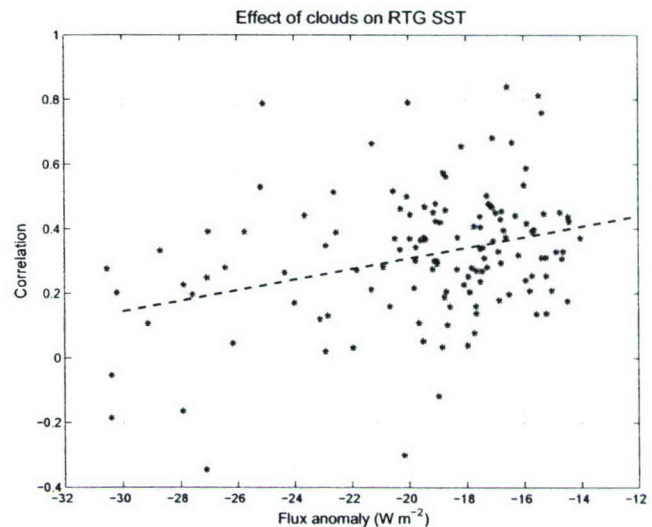
**Figure 13.** As in Figure 12, except TMI SST.

Figure 15. Effect of cloudiness on temperature tendency. Scatter plot of correlations between temperature tendency from RTG and from microwave SST (as a proxy for RTG accuracy) versus shortwave flux anomalies (as a proxy for cloud cover). The regression line (dashed) between the proxy for RTG SST accuracy and the proxy for cloud cover.

A visual inspection of the heat fluxes and winds showed no obvious anomalies in 2002. Correlations between model and SST products using the NCEP2 versus the NCEP2/COARE net surface heat flux products are nearly identical, suggesting that different flux products are not an important factor in the differences in correlations.

To examine the possibility that the model may be performing well, but that the SST used for the evaluation is not uniformly accurate, correlations were also performed using the TMI SST in the regions in which it is available (Figure 13). Again, correlations are significant over much of the region for most years; however, the regions and years of high correlations differ from those using RTG. Typically, correlations of the model $\partial T/\partial t$ are higher with TMI than with RTG SST.

The RTG product is derived from infrared data, which is readily contaminated by clouds, whereas the coarser microwave data has significant errors only when it is raining or near land (as discussed above). A simple indicator of the level of cloudiness can be obtained from the shortwave radiation from ISCCP, which decreases substantially in the presence of clouds. The effect of clouds on the model/SST comparisons is examined more closely at one location (36.5°N, 18.5°E) in the central Mediterranean (Figure 14). Correlations of model $\partial T/\partial t$ with the TMI $\partial T/\partial t$ are above 0.5 in all years except 2003, whereas the correlations with the RTG $\partial T/\partial t$ are only significant in 2001. For this location the temperature tendency from each SST product and from the mixed layer model are plotted in Figure 14 (left column) for each year. In the right column are plotted the shortwave flux anomalies from the seasonal cycle. There are relatively large negative anomalies (large

cloud contributions) except in year 2001, the only year in which RTG compares well with the model. This example suggests that cloudiness may be responsible for lower correlations between the model and RTG $\partial T/\partial t$.

The effect of cloudiness on infrared SST tendency can be estimated. If the clouds are significantly degrading the RTG SST (but not the microwave SST), one would expect poor correlations between the two SST products during cloudy periods (Figure 15). For the central Mediterranean (33.5–37.5°N, 15.5-21.5°E) where the apparent model accuracy differs greatly between the two SST products, correlations between $\partial T/\partial t$ from RTG and TMI are plotted against the average anomalies of shortwave flux for 15 October - 15 December of each year. From the plot it can be seen that low correlations of RTG with TMI SST coincide with negative flux anomalies (cloudiness), indicating that errors from cloud contamination in the RTG product are significantly reducing its usefulness for evaluating model performance.

Thus, the TMI SST is a better indicator of model performance than RTG, where the data are available and are not influenced by nearby land. In the Aegean Sea, where TMI data are masked out by land, the model performs quite well in all four years, suggesting that cloud contamination of RTG SST may be less of a prob-
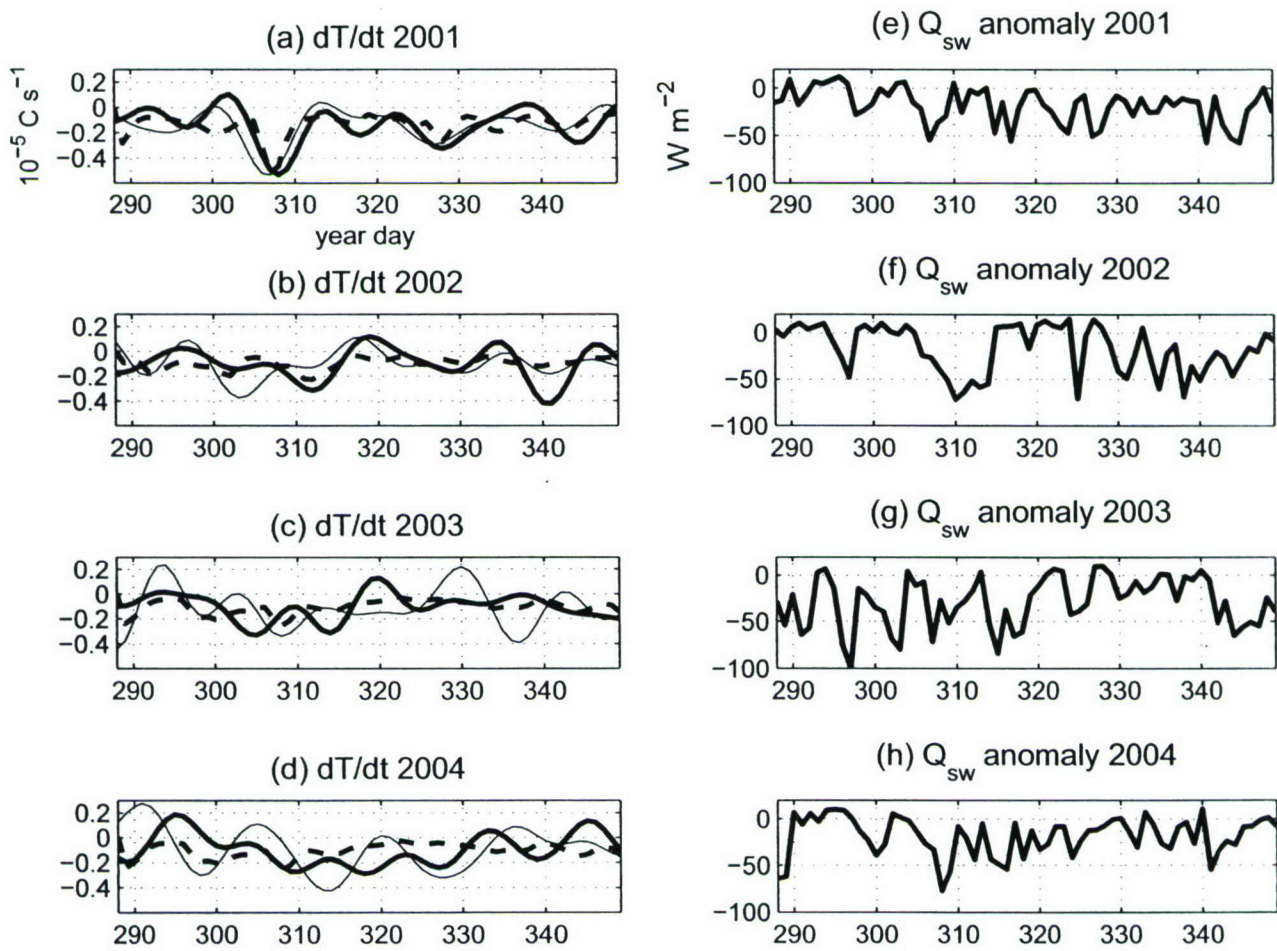
Figure 14. Temperature tendency and shortwave flux anomalies at 36.5°N, 18.5°E. Temperature tendency from RTG (thin line), from microwave SST (thick line), and from the mixed layer model (dashed line) for the fall of (a) 2001, (b) 2002, (c) 2003, and (d) 2004. (e)-(h) Anomalies from seasonal cycle of shortwave radiation for fall of the same four years.

lem there.

4.2. Mixed Layer Temperature Variability

The PWP model shows substantial variations in mixed layer temperature (MLT) variability on time scales of about 10–14 days. (Recall that variability on time scales shorter than about 9 days has been removed from the SST data, as described in Section 2.3). These changes could be caused by variations in heat flux, in wind forcing, or mixing. In addition, the column mixed layer model neglects temperature advection from both Ekman and geostrophic current components.

To determine the extent of the various processes to $\partial T/\partial t$, each of the forcing functions in turn was low-pass filtered (half-power of 30 days), while the others retained daily variations. A location and year in which the correlations with both RTG and TMI were relatively high was selected: 33.5°N, 27.5°E in 2003. The correlation between model and observations was 0.65 for the baseline run (Figure 16a). Removing the high-frequency fluctuations in wind stress, wind stress curl, or shortwave radiation had a negligible effect on the correlations with TMI. However, removing high-frequency fluctuations from the turbulent fluxes (actually the turbulent plus longwave fluxes, but longwave fluxes are quite small) removed nearly all the variability in the model $\partial T/\partial t$, reducing the correlation to 0.39 (Figure 16b).

The comparison of the model and observed $\partial T/\partial t$ in Figure 16a is fairly typical in that the model slightly underestimates the magnitudes, even at the beginning of the run when model MLD agrees well with climatology. Near the end of the run, at many locations, MLD is overestimated, resulting in even smaller $\partial T/\partial t$ magnitudes, relative to observed values. These comparisons suggest that the energetic NCEP2 turbulent fluxes are more consistent with observed SST changes than the NCEP2/COARE fluxes.

The PWP model run independently at each grid point neglects horizontal processes (advection and diffusion) that might significantly affect the mixed layer temperatures. Experiments were performed to estimate the effects of temperature advection in the mixed layer. To estimate the effect of horizontal advection by the Ekman response to winds, the modeled Ekman velocity was combined with observed SST gradients (assuming a uniform horizontal temperature gradient with depth over the Ekman layer) and compared with the model run without advection. The difference at several grid points showed a relatively small contribution, a warming or cooling of about 0.1-0.2°C over the 3-month period. Correlations between modeled and ob-
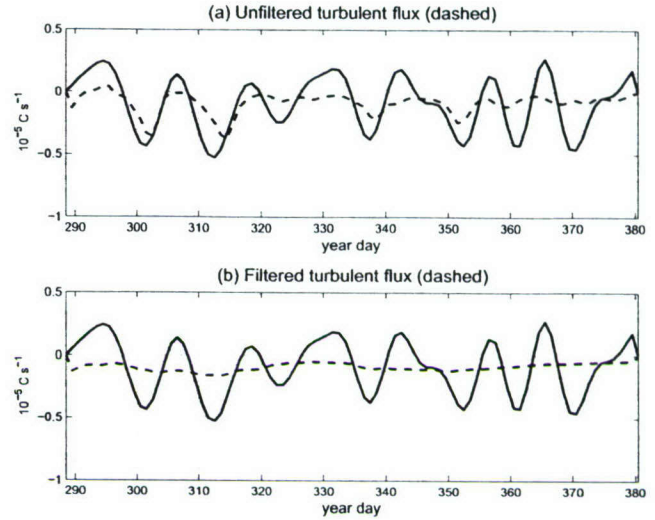
Figure 16. Source of high frequency variations in mixed layer temperature. Temperature tendency $\partial T/\partial t$ at 33.5°N, 27.5°E in fall of 2003 from (a) TMI SST (solid line) and model run with daily forcing (dashed line) and from (b) model run with smoothed version of turbulent heat fluxes (dashed line). Observed SST repeated in (b) (solid line). Units are °C s^{-1}.

served $\partial T/\partial t$ were not significantly changed. The PWP model does not include geostrophic currents. Hypothetically, these could be estimated using geostrophic velocity anomalies from the altimeter; however, a mean sea surface for the Mediterranean Sea is not readily available to supplement the anomalies.

Currents were available at 3-m depths at the buoys in the Aegean Sea, although there were substantial data dropouts during the study period. A nearly complete record for the fall of 2002 at the Santorini buoy (Figure 17) was used to examine the effect of Ekman plus geostrophic advection. The observed daily-averaged currents resemble the modeled Ekman currents, but the time series are only marginally correlated. The modeled currents do not have the observed lower frequency (>10-day periods) fluctuations, which presumably are the geostrophic component. The effect of advection on model accuracy by the observed currents is quantified (Table 2) using correlations between model and 3-m buoy temperature tendency and between the model and RTG SST tendency. Adding advection increased (buoy) or decreased (RTG) correlations somewhat, but these changes are relatively small. Again, this shows that the PWP column model is doing fairly well in hindcasting MLT.
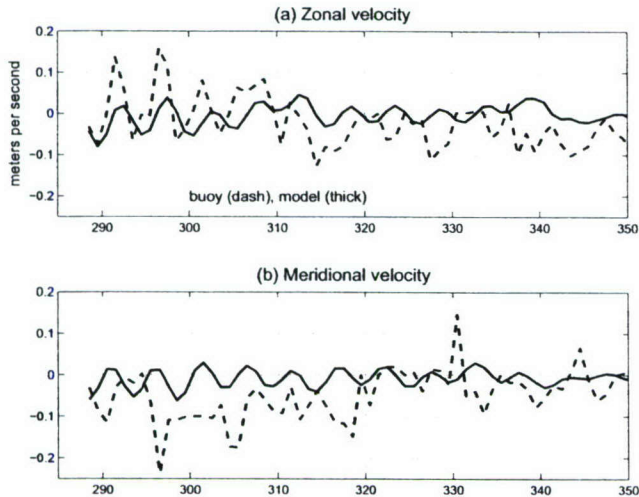
Figure 17. Observed and modeled currents at Santorini.(a) zonal and (b) meridional currents from buoy (dashed) and model (solid).

Table 1. Correlations of $\partial T/\partial t$ with and without advection at Santorini

	RTG SST	Buoy 3-m
No advection	0.59	0.60
Advection	0.51	0.63

4.3. Effect of Wind Accuracy

As noted in Section 4.2, wind stress and wind stress curl have little direct effect on the prediction of SST using the model, compared with the effects of turbulent heat fluxes. However, wind speed likely makes a large contribution to the NCEP2 turbulent fluxes, and poor spatial resolution in wind speed may have a large effect on SST through the turbulent fluxes. Wind speeds near the numerous islands in the Mediterranean Sea are highly variable spatially, owing to the complex topography, and are not resolved by the NCEP2 Reanalysis product.

To study the effect of poor spatial resolution in wind speed on the NCEP2 turbulent flux products, and in turn on model accuracy, a region south of the island of Crete was selected for further study. High-resolution fields of wind speed derived from the QuikSCAT data (Figure 1b) show variability on spatial scales much smaller than the resolution of the NCEP2 flux products; these differences are sufficiently robust that they can be seen in the standard deviation of the November-December-January wind speeds for 2001–2004 (Figure 18). Note the local minimum in wind speed variations south of central Crete (35°N, 25°E) where the
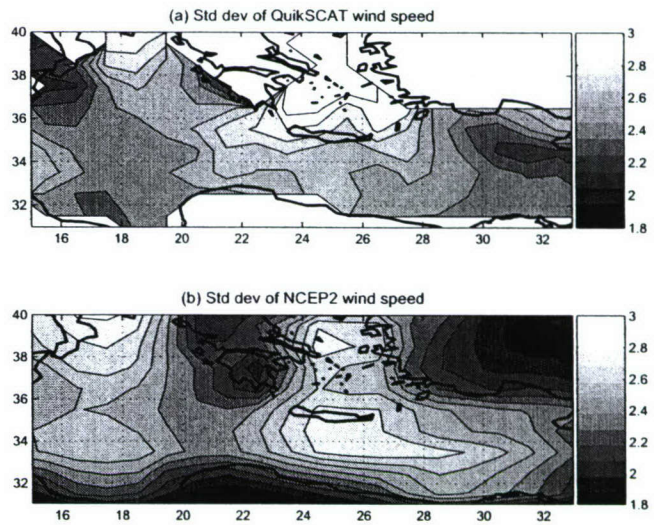

Figure 18. Standard deviation of wind speeds for November-December-January. (a) QuikSCAT and (b) NCEP2 in units of $m\,s^{-1}$.

topography blocks the prevailing northerly winds. The QuikSCAT wind fields used here, although mapped to the same 1° grid as the NCEP2 products, have true 1° resolution, whereas the winds (and the other variables) used in the NCEP2 and NCEP/COARE products are much smoother.

To characterize the accuracy of the NCEP2 fluxes, correlations were performed between the NCEP2 and QuikSCAT winds along 34.5°N from 19.5–32.5°E for each of the four years of the study, on the assumption that locations where NCEP2 winds are more highly correlated with the QuikSCAT winds have more accurate flux estimates than locations with low correlations. This proxy for flux field accuracy was then compared with a measure of model accuracy, the correlation between observed and model temperature tendency $\partial T/\partial t$ (Figure 19). A regression between the two correlations gives the best-fit line (dashed line in Figure 19) with a correlation of 0.41, which is just significant at 95% confidence. This analysis gives an estimate of the degradation in model performance (a drop in correlations as large as 0.2) that results from poorly resolved spatial variations in the flux products.

4.4. Characterizing Model Accuracy

In Section 4.1 the correspondence between model and observed temperature tendency was characterized using correlations. One drawback of the use of a correlation is that it does not include any measure of the relative magnitudes of the model and the observed fluctuations, and therefore, hides an under- or over-prediction. For
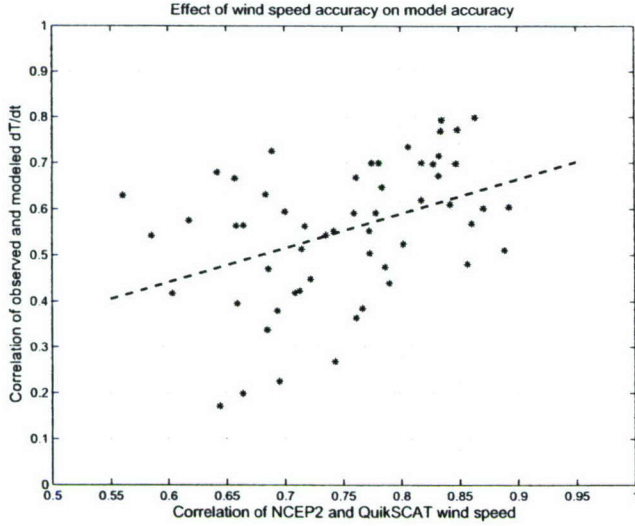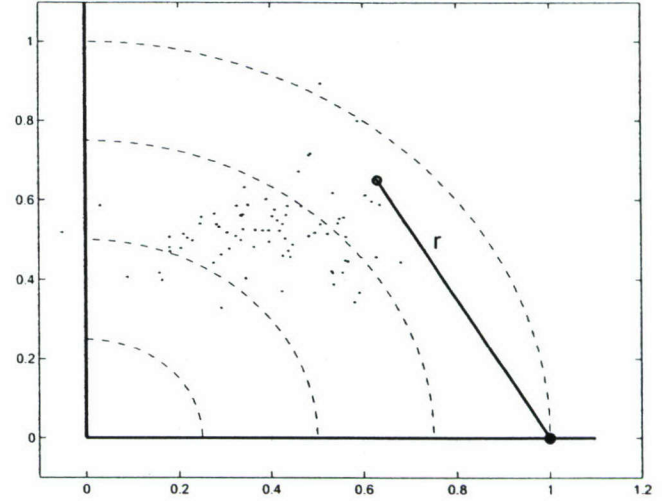
Figure 19. Effect of wind speed accuracy on model accuracy. Correlations between observed and modeled temperature tendency $\partial T/\partial t$ versus correlations between NCEP2 and QuikSCAT wind speed south of Crete.

Figure 20. Example of a normalized Taylor diagram. Using polar coordinates, the ratio of the standard deviations of model and observed temperature tendency (radial coordinate) and the correlation angle θ are plotted for each location and each year. The normalized error is the distance r from each point to the location of a perfect correlation (on the x-axis) and a ratio of one. See text for explanation.

example, the difference in the magnitudes of the latent heat flux anomalies of NCEP2 versus NCEP2/COARE, as shown in Figure 7, along with the sensitivity of the model to latent heat flux anomalies, suggests that the magnitude of the model's response should be larger for NCEP2. Correlations with observed temperature tendency for the model forced with the two flux products were nearly identical and give no indication of which product gives smaller errors. An additional problem is that a correlation between model and observations can be increased by filtering the model input (or output) to remove higher-frequency (uncorrelated) variations without actually improving the model performance. The filtering may result in under-prediction by the model, but this effect will not be measured with a correlation. Thus, a correlation is not an ideal method of evaluation.

An alternative method to describe model accuracy is the so-called Taylor diagram [*Taylor*, 2001]. Polar coordinates are used to plot both correlation (θ) and magnitudes (r). Here, the normalized version of this diagram is used, so that the root-mean-square (rms) ratio of the modeled values to the observed values is plotted as the radial distance from the origin (Figure 20). The angle with respect to the x-axis is derived from the correlation, as

$$\theta = cos^{-1}\rho$$

so that a perfect correlation lies along the x-axis and a

zero correlation lies along the y-axis. The center of the cluster of points in the figure lies at a magnitude ratio of about 0.6 and correlations of about $\rho = 0.66$.

The distance of any point from the intersection of the circle of radius one and the x-axis is a normalized measure of the accuracy of the model prediction of temperature tendency; the distance is the ratio of the standard deviation of the error, divided by the standard deviation of the signal, here, the observed value of $\partial T/\partial t$. In Figure 20 the error r shown is about 0.75, which means at this location in this year, the PWP model has an error of about 75% of the standard deviation of observed $\partial T/\partial t$. For $r > 1$ the model error would exceed the signal and the model has no useful skill in simulating $\partial T/\partial t$.

Normalized errors using COARE versus NCEP2 heat fluxes (not shown) are approximately 10% more in the central Mediterranean, a clear indication of an under-prediction of temperature tendency by COARE there. The use of $\partial T/\partial t$ as a metric for evaluating the model is quite stringent and, therefore the normalized distances are large. Clearly the model simulates MLT well (for example, Figure 11a) and a metric based on $T(t)$ would likely have much smaller normalized errors.

The measurements of error in Figure 21 use the SST product that gives the smallest normalized errors over
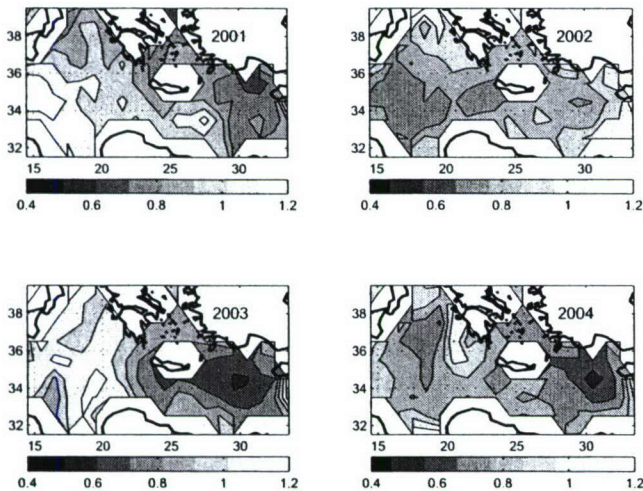
Figure 21. Evaluation of model using Taylor diagram. Normalized errors in temperature tendency by the model relative to the best SST observation.

all four years (compare with Figure 12 and 13). Generally, the TMI SST is used for the interior points and RTG SST is used near land. A distance of 1.0 indicates where the expected model error is the same size as the standard deviation of $\partial T/\partial t$, that is, where the PWP model has no useful skill in predicting MLT variations. The regions of largest (relative) errors are the central Mediterranean Sea, the western part of the study region.

5. Summary and Conclusions

The goal of this study is to determine whether available observations can be used to determine when an ocean model is missing essential physics, specifically, whether mixing processes not represented in a mixed layer model are responsible for systematic temperature prediction biases. At this point, errors in forcing fields and comparison temperature data make that determination difficult. Based on the analyses here, the model appears to be performing well compared with the available observations, in that times and locations of poor model performance generally correspond to poor quality of forcing or observed SST fields. For example, poor model performance, as judged by correlations with temperature tendency from the RTG SST product, correspond to periods of heavy cloud cover or to regions where spatial resolution in air-sea fluxes is inadequate.

On the other hand, it appears that the model can help determine which of the available observations and forcing fields are most accurate. For example, the microwave SST gave consistently higher correlations with

the model than the infrared-based RTG product, except near land where there is a warm SST bias in the microwave data. The accuracy of the infrared product is degraded in periods of high cloud cover (Figure 15), as parameterized by negative shortwave flux anomalies. Large corrections to the freshwater fluxes (in the sense of increasing the precipitation) are required for consistency with climatological salinity, suggesting that these fluxes have little useful skill for forcing the model.

NCEP2 heat fluxes, which have the largest temporal variations of the flux fields examined here, still underestimate the variations in temperature tendency (Figure 16). Part of the underestimate comes from an overestimate of mixed layer depth; however, the underestimate is apparent even at the beginning of the model runs, when the MLD is very near its climatological value and occurs at locations where MLD matches climatology well throughout the run, as in Figure 16. NCEP2 radiative fluxes have temporal variations about twice as large those from ISCCP and temporal variations in turbulent fluxes about 40% larger those made by using NCEP2 daily fields in the COARE algorithm. The COARE algorithm is designed to produce realistic fluxes using hourly input fields, rather than the daily values used here, which could account for the underestimate; however, a recent analysis by [*Jiang et al.*, 2005] suggests that the COARE algorithm is not highly nonlinear.

The source of the high-frequency temperature fluctuations was determined using a series of model experiments and comparing the results with observations. At the highest frequency resolved by the observed SST (periods of about 9 days) variations in SST are caused by corresponding variations in turbulent heat fluxes. No other forcing field examined (shortwave radiation, wind stress, freshwater fluxes) makes a significant contribution. Advection makes only a small contribution to the SST tendency in the Aegean Sea, the only location where currents are available.

As expected from the importance of the turbulent heat flux, errors in the flux estimates appear to degrade model performance. In the region south of Crete, where QuikSCAT winds show large topographic effects at small scales, the coarse resolution of NCEP2 flux fields appears to significantly degrade model results. Using the correlation of NCEP2 and QuikSCAT wind speeds (Figure 19) as a measure of NCEP2 turbulent flux accuracy, regions of poor NCEP2 flux accuracy correspond to regions of poor model performance.

Model accuracy is characterized using correlations of observed and modeled temperature tendency, to emphasize the highest frequencies resolved by the observa-

tions (periods of 9 days or more). To include information about over- or under-prediction of the temperature tendency, normalized errors are computed based on the Taylor diagram. This characterization reveals that the PWP model (forced by currently available fields) has its greatest skill in predicting temperature tendency in the eastern part of the study region, and has no useful skill in the central Mediterranean (15°E– 20°E), the westernmost part of the study region. Further, it shows that the larger NCEP2 flux anomalies give better results than the other flux products tested, particularly in the eastern Mediterranean. Skill in modeling temperature, rather than temperature tendency, is expected to be much greater.

The new satellite products (microwave SST and scatterometer winds) clearly have the potential to improve both forcing and comparison fields, to allow an examination of shortfalls in model physics. However, consistent high-spatial-resolution SST and flux products need to be derived from the new data fields to allow interpretation of poor model performance as missing or inaccurate model physics. A new SST product (GHRSST from GODAE) combining infrared, microwave, and in situ temperatures will soon be available, as will a higher resolution (12.5km) wind product from the QuikSCAT scatterometer. As suggested by the analysis here, these products may make possible the detection of shortcomings in model physics by careful comparison with observations.

References

Cazenave, A., C. Cabanes, K. Dominh, and S. Mangiarotti) (2001), Recent sea level change in the Mediterranean Sea revealed by Topex/Poseidon satellite altimetry. *Geophys. Res. Lett.*, *28*(8), 1607–1610.

Chelton, D.B., M.G. Schlax, M.H. Freilich, and R.F. Milliff, (2004), Satellite measurements reveal persistent small-scale features in ocean winds, *Science*, *303*, 5660, 13 Feb. 2004, 978-983.

Conkwright. M.E., J.I. Antonov, O. Baranova, T.P. Boyer, H.E. Garcia, R. Gelfeld, D. Johnson, R.A. Locarnini, P.P. Murphy, T.D. O'Brien, I. Smolyar, and C. Stephens, (2002), *World Ocean Database 2001, Volume 1: Introduction.*, Ed. Sydney Levitus, NOAA Atlas Nesdis 42, U.S. Government Printing Office, Washington, D.C., 167 pp.

Fairall, C.W., E.F Bradley, D.P. Rogers, J.B. Edson, and G.S Young, (1996), Bulk parameterization of air-sea fluxes for Tropical Ocean-Global Atmosphere Coupled-Ocean Atmosphere Response Experiment *J. Geophys. Res.*, *101*, 1996, 3747-3764.

Fukumori, I., D. Menemenlis, and T. Lee, (2006), A Near-Uniform Basinwide Sea Level Fluctuation of the Mediterranean Sea, *J. Phys. Oceanogr.*, in press.

Ivanov, A. Yu., (2002), ALMAZ-1 SAR and ERS-1 SAR in oceanographic applications: a final assessment, Proceedings 4th European Conference on Synthetic Aperture Radar. EUSAR 2002, p 741.

Global Ocean Associates, "An atlas of internal solitary-like waves and their properties," Second edition, February 2004, Prepared under contract with the Office of Naval Research, Code 322PO, http://www.internalwaveatlas.com/Atlas2_index.html

Jiang, C., M. Cronin, K. A. Kelly, and L. Thompson, (2005), Evaluation of a hybrid satellite and NWP based turbulent heat flux product using TAO buoys. *J. Geophys. Res.*, *110*, C09007, doi:10.1029/2004JC002824.

Kelly, K. A., S. Dickinson, and Z.-J. Yu, (1999), NSCAT tropical wind stress maps: Implications for improving ocean modeling, *J. Geophys. Res.*, *104*, 11,291–11,310.

Kistler, R., E. Kalnay, W. Collins, S. Saha, G. White, J. Woollen, M. Chelliah, W. Ebiszaki, M. Kanamitsu, V. Kousky, H. van den Dool, R. Jenne, and M. Fiorino, (2001), The NCEP-NCAR 50-Year Reanalysis: MonthlyMeans CD-ROM and Documentation. *Bull. Amer. Meteor. Soc.*, *82*, 247–268.

Krahmann, G. and F. Schott, (1998), Longterm increases in Western Mediterranean salinities and temperatures: anthropogenic and climatic sources, *Geophys. Res. Lett.*, *25*, (22), 15 Nov. 1998, 4209–4212.

Krahmann, G. F. Schott, and U. Send, (2000), Seasonal heat content change in the western Mediterranean Sea as a means for evaluating surface heat flux formulations. *J. Geophys. Res.*, *105*, 16941–16,950.

Matteoda, A. M., and S. M. Glenn, 1996) Observations of recurrent mesoscale eddies in the eastern Mediterranean, *J. Geophys. Res.*, *101*, 20687–20709.

Pinardi, N., G. Korres, A. Lascaratos, V. Roussenov, and E. Stanev, 1997) Numerical simulation of the interannual variability of the Mediterranean Sea upper ocean circulation, *Geophys. Res. Lett.*,*24*, 425–428.

Price, J.F., R.A. Weller, and R. Pinkel, 1986. Diurnal cycling: observations and models of the upper ocean response to diurnal heating, cooling, and wind mixing *J. Geophys. Res.*, *91*, 8411–8427.

Poulos, S.E., P.G. Drakopoulos, and M.B. Collins, 1997) Seasonal variability in sea surface oceanographic conditions in the Aegean Sea (Eastern Mediterranean): an overview, *J. Mar. Systems*, *13*, 225–244.

Reynolds, R. W., and T. M. Smith, 1994) Improved global sea surface temperature analyses using optimal interpolation, *J. Climate*, *7*, 929–948.

Sofianos, S., W. Johns, A. Lascaratos, S. Murray, D. Olson, and A. Theocharis, 2002) Draft Report of the Aegean Sea Workshop, Rhodes, Greece, 8-10, 2002, www.oc.phys.uoa.gr/workshop/ Aegean_Draft_Report_f.htm.

Taylor, K.E., 2001) Summarizing multiple aspects of model performance in a single diagram, *J. Geophys. Res.*, 106, 7183–7192.

Vignudelli, S., G. P. Gasparini,M. Astraldi, M. E. Schiano, 1999) Possible influence of the North Atlantic Oscillation on the circulation of the Western Mediterranean Sea, *Geophys. Res. Lett.*, *26*(5), 623–626.

Zhang, Y., W. B. Rossow, A. A. Lacis, V. Oinas, and M. I. Mishchenko (2004)) Calculation of radiative fluxes from the surface to top of atmosphere based on IS-CCP and other global data sets: Refinements of the radiative transfer model and the input data, *J. Geophys. Res.*, *109*, D19105, doi:10.1029/2003JD004457.

Kathryn A. Kelly, Applied Physics Laboratory, University of Washington, Box 355640, Seattle, WA, 98195-5640,USA. (kkelly@apl.washington.edu)